processes

MDPI

Article

Dynamic Impedance Model of Low-Voltage Electric Shock in Animals Considering the Influence of Water Electrolysis

Haixin Tong, Xiangjun Zeng, Kun Yu * and Zehua Zhou

State Key Laboratory of Disaster Prevention and Reduction for Power Grid, Changsha University of Science and Technology, Changsha 410114, China; tonghaixin@stu.csust.edu.cn (H.T.); eexjzeng@csust.edu.cn (X.Z.); zhouzehua@stu.csust.edu.cn (Z.Z.)
* Correspondence: kunyu0707@163.com

Abstract: This study aims to tackle the challenge of explaining the underlying mechanisms behind the time-varying impedance phenomenon in animals experiencing low-voltage electric shocks. A dynamic impedance model that considers the effect of water electrolysis (WEDI) has been developed. First, we conducted root cause analyses through progressive validation experiments, identifying water within the shocked body as the key factor influencing impedance variation. Monitoring hydrogen concentration above the electrodes and measuring mass changes in the shocked body revealed that the time-varying impedance is closely related to internal water electrolysis. Second, we quantitatively analyzed the impact of water molecule decomposition during electrolysis on the salt concentration and conductivity within the electrically shocked body. A mathematical relationship between the variable resistance within the body and time was derived. A dynamic impedance model for animal electric shock that considered the effects of water electrolysis was subsequently established, explaining the underlying mechanism behind the time-varying impedance phenomenon. Finally, the Mean Absolute Percentage Error (MAPE), Mean Absolute Error (MAE), and Root Mean Square Error (RMSE) between the electric shock current predicted by the WEDI model and actual measurements were 0.00357, 0.00350, and 0.00446. Compared to existing models, the WEDI model demonstrates superior accuracy and interpretability.

Keywords: dynamic impedance model; electrically shocked body; low-voltage; water electrolysis

Citation: Tong, H.; Zeng, X.; Yu, K.; Zhou, Z. Dynamic Impedance Model of Low-Voltage Electric Shock in Animals Considering the Influence of Water Electrolysis. *Processes* **2024**, *12*, 2565. https://doi.org/10.3390/pr12112565

Academic Editor: Pavel Mokrejš

Received: 3 October 2024
Revised: 4 November 2024
Accepted: 14 November 2024
Published: 16 November 2024

1. Introduction

Electric shocks in low-voltage systems are serious accidents. Victims cannot easily break free and can be in life-threatening danger quickly. In China, the annual death toll from electric shock accidents reaches as high as 8000 [1]. Approximately 70% of these electric shock incidents occur in low-voltage distribution networks [2]. With the increasing demand for electricity, there are growing expectations for the safety of distribution networks [3–5]. The animal body impedance model is the foundation of electric shock protection technology. Developing an accurate model to precisely describe current changes during shocks is crucial for personal protection and the safe, stable operation of the power grid.

As early as the first half of the last century, researchers proposed classic human equivalent circuit models based on the electrical equivalence of the human body: the Freiberger model and the Biegelmeier model [6]. Later, to standardize the models used by researchers, the International Electrotechnical Commission (IEC) held an academic conference in 1987 and established a more authoritative human impedance model [7]. The approach to constructing the aforementioned model is as follows: parts of the organism with higher electrical conductivity (such as various organs, bodily fluids) are equivalently represented as resistors, while parts with lower conductivity (such as the stratum corneum of the skin) are equivalently represented as capacitors. These resistors and capacitors are then adaptively combined based on real-world scenarios.

In subsequent research, this approach has also become the mainstream concept for bio-impedance modeling and is widely applied in various fields of study [8,9]. At the same time, these models are continuously optimized according to the needs of different application scenarios. De Santis et al. [10] addressed the challenge that traditional models have difficulty replicating the electrical behavior of human impedance at high frequencies. They proposed an equivalent circuit that accurately describes the variation pattern of human impedance under voltage in the frequency range from 40 Hz to 110 MHz. Chinen et al. [11] proposed an impedance model composed of five parallel high-pass RC branches to accommodate a more precise armpit electrode method for measuring human impedance, which helps improve the accuracy of bioimpedance measurements. Bora et al. [12] proposed a hybrid model that combines a fractional-order constant phase element (CPE) and high-order resistance capacitance (RC) based on the characteristics of different types of skin, achieving more accurate human skin impedance modeling. Freschi et al. [13] developed a complex resistor–capacitor combination model to study human behavior under the influence of an electric field. Ferreira et al. [14] applied an electrical skin model to explain the impedance data of human and rabbit skin under stimulated conditions. Li et al. [15,16] used finite element technology to create a 3D model of pigs, achieving a more accurate impedance model. These studies have improved the accuracy of the models to a certain extent, but the bio-impedance models they used are inadequate in describing the nonlinear characteristics of the equivalent circuit when biological tissues experience electric shock.

To approach this difficulty, some researchers have conducted related work. Dorgan et al. [17] studied the nonlinear characteristics of skin impedance under DC voltage and proposed a mathematical model to describe the variation of skin impedance under DC voltage. Pritchard et al. [18] proposed a mathematical model addressing the voltage-dependent characteristics of human impedance, providing a more accurate description of the relationship between human impedance and voltage. Yang et al. [19] developed a mathematical model to describe the phenomenon of time-varying bio-impedance after electric shock, providing a more accurate depiction of the changes in impedance of shocked animals. These models can describe the nonlinear characteristics of bio-impedance under electric current, but their core modeling approach is based on numerical fitting to experimental data. They still struggle to explain, from a mechanistic perspective, the phenomenon of waveforms unique to biological electric shocks, in which animal impedance decreases and then gradually stabilizes during the electric shock.

In response to the above problem, this paper establishes a dynamic impedance model of animal body considering the impact of water electrolysis (WEDI). The main contributions of this paper are as follows:

- Qualitative analysis is conducted. The key factors for the phenomenon of waveforms unique to biological electric shocks are traced. The relationship between this phenomenon and water electrolysis reactions is explored. The mechanism of impedance evolution in electrically shocked bodies is revealed;
- A new model is established. The mathematical relationships among the water molecule content, solution concentration, conductivity, and the resistance of the electrically shocked body during the electrolysis of water have been quantitatively analyzed. On this basis, an interpretable impedance model of the animal body is established, enabling accurate calculation of the dynamic impedance in the electrically shocked animal body;
- Experimental validation is conducted. The validity of the proposed WEDI model is verified using measured data from live animal electric shock experiments. Comparative analysis with three commonly used bio-impedance models demonstrates that the WEDI model not only achieves higher accuracy but also provides better interpretability.

The remainder of this paper is organized as follows. Section 2 reveals the mechanism behind the time-varying impedance phenomena in electrically shocked bodies. Section 3 proposes a dynamic impedance model of the animal body that considers the impact of

water electrolysis. Section 4 conducts experimental validation of the proposed model using a real-world testing platform. Section 5 concludes the paper.

2. The Mechanism of Time-Varying Body Impedance Phenomenon During Electric Shock

In the initial stages of electric shock, the impedance of an animal's body exhibits time-varying characteristics. As shown in Figure 1, the waveform is derived from real-time data collected from live mice during electric shock in our lab. The voltage waveform during electric shock is a sinusoidal wave with a constant amplitude. The current amplitude shows a significant increase during the first three cycles and then gradually stabilizes, indicating that the magnitude of the animal's body impedance transitions from higher to lower values before stabilizing. This waveform is a typical phenomenon of biological electric shocks and is referred to as "waveforms unique to biological electric shocks". We have thoroughly investigated the key factors that lead to the time-varying impedance phenomenon in electrocuted objects and have qualitatively described this phenomenon.

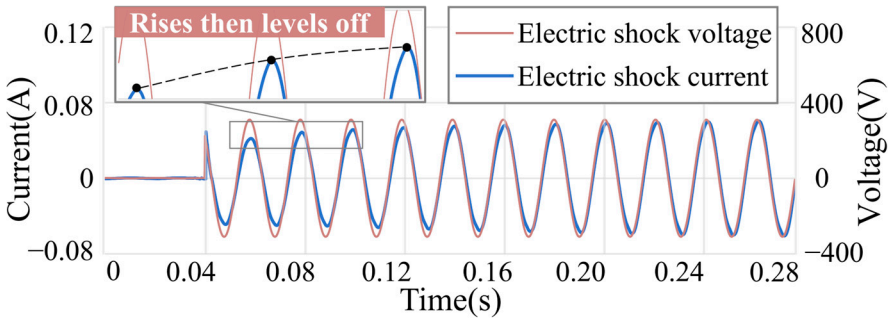

Figure 1. Waveform diagram of current and voltage during electric shock to a live body.

2.1. Traceability Analysis of Key Factors for Time-Variant Impedance Phenomena

The analysis approach for tracing key factors of time-variant impedance phenomena in animal bodies is shown in Figure 2. First, the relationship between the time-variant phenomenon of waveforms unique to biological electric shocks and the life activities of a living organism is verified. The data of a living animal under electric shock (as shown in Figure 1) are compared and analyzed with the data of a non-living piece of raw meat under electric shock (as shown in Figure 3). The moment of electric shock occurs at 0.04 s. Under the condition that the voltage amplitude of the electric shock is stable, the current amplitude of both the living animal and the non-living raw meat shows a gradual increase followed by stabilization. This indicates that the equivalent impedance of both decreases initially and then stabilizes during the early stage of electric shock. Therefore, it can be concluded that the phenomenon of body impedance decreasing and then stabilizing upon electric shock is unrelated to the life activities of the living organism.

Based on the intermediate conclusion that the studied phenomenon was unrelated to the activities of living organisms, we continued to verify the relationship between the time-varying impedance during electric shock and meat tissue materials. Thus, we needed to introduce a material that could replace meat tissue for a control experiment. Since meat consists of porous tissue material filled with an aqueous solution, we replaced it with a porous wooden block. The wood was thoroughly soaked in saltwater before conducting the electric shock experiment. We compared the data from the wooden block during electric shock (Figure 4) with that from raw meat during electric shock (Figure 3). Under constant voltage amplitude, the saltwater-soaked wood also exhibited a trend where the current amplitude initially increased and then stabilized, indicating that its equivalent impedance underwent a change from high to low before stabilizing. This suggested that the time-varying impedance phenomenon of waveforms unique to biological electric shocks was not related to meat tissue materials.

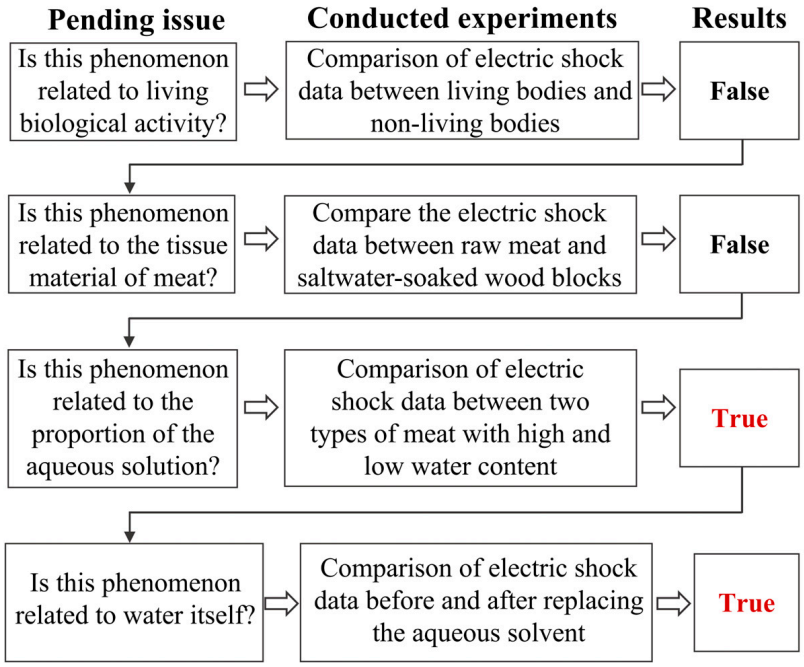

Figure 2. A concept map for the trace analysis of key factors in impedance time-variation phenomena. The red font is used to highlight positive results, while black font indicates negative results.

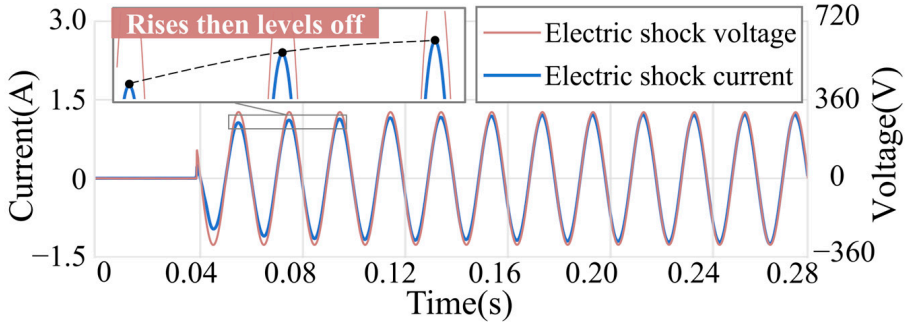

Figure 3. Waveform of current and voltage from electric shock to raw meat (approximately 75% water content).

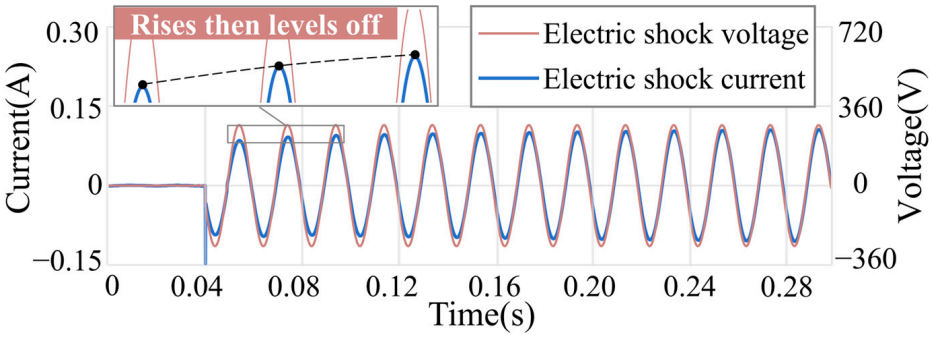

Figure 4. Current and voltage waveform of saltwater-soaked wooden block during electric shock.

Based on the intermediate conclusion that the phenomenon of waveforms unique to biological electric shocks being studied was unrelated to the material of meat tissue, we continued to verify the relationship between this phenomenon and the proportion of aqueous solution in the body subjected to electric shock. Therefore, it was necessary to observe the data of raw meat with relatively low water content subjected to electric shock. As shown in Figure 5, when the voltage amplitude of the electric shock remained constant, there was no

significant increase in current amplitude for raw meat with lower water content (about 6%) compared to the raw meat in Figure 3 (about 75% water content). In the data for raw meat with lower water content, it was difficult to observe the phenomenon of waveforms unique to biological electric shocks. Thus, it was concluded that this phenomenon was related to the proportion of aqueous solution in the meat.

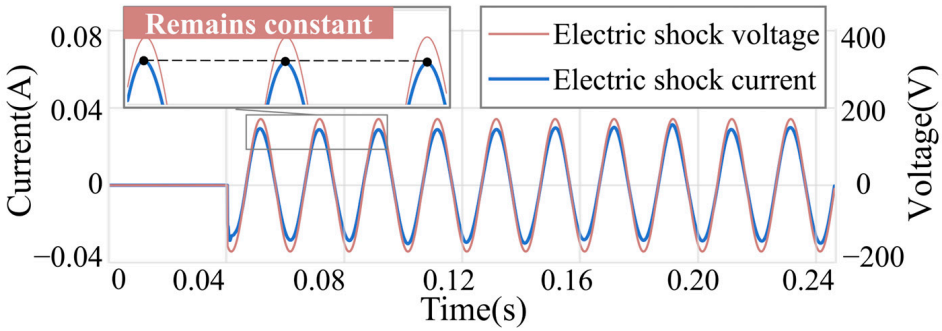

Figure 5. Waveform diagram of current and voltage for raw meat with lower water content (approximately 6% water content) subjected to electric shock.

Based on the premise that the phenomenon being studied was related to the proportion of aqueous solution, we further verified the relationship between this phenomenon and the solvent water itself. It was known that wood soaked in saltwater exhibited the phenomenon of waveforms unique to biological electric shocks. We replaced the solvent in the saltwater with glycerol, which could dissolve sodium chloride, creating a glycerol solution of sodium chloride. A piece of wood was then soaked in this solution. After the solution had fully permeated the wood, an electric shock test was conducted. The experimental data are shown in Figure 6. Under the condition that the voltage amplitude of the electric shock remained stable, there was no significant increase in the current amplitude. Based on the disappearance of the studied phenomenon after replacing the solvent water, it was concluded that the phenomenon of the body's impedance decreasing from high to low and then stabilizing was related to the solvent water.

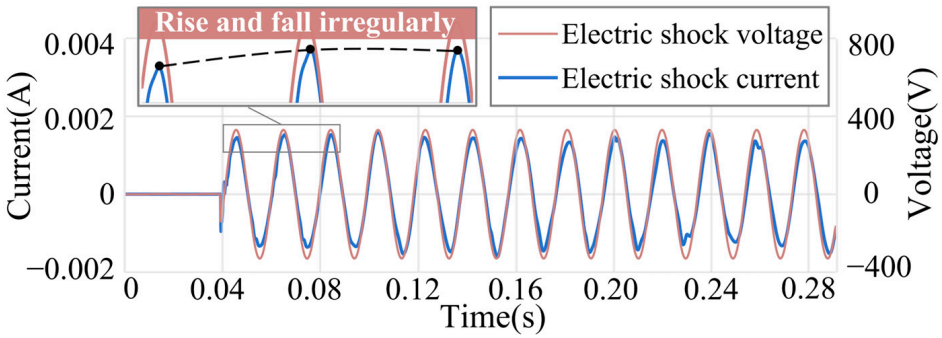

Figure 6. Waveform diagram of current and voltage for wood that has been soaked in glycerol solution of sodium chloride and then subjected to electric shock.

Moreover, we have compiled a table summarizing the relationships between different materials and their key phenomena, as shown in Table 1. From this information, it is evident that materials with higher moisture content demonstrate the waveforms unique to biological electric shocks, whereas those with lower moisture content do not. Additionally, based on the relationships observed, we can exclude the possibility that this phenomenon arises from biological activity, meat tissue materials, or salt ions. In conclusion, we determine that the waveforms unique to biological electric shocks is associated with water.

Table 1. Relationship table between experimental materials and the phenomenon of waveforms unique to biological electric shocks.

Experimental Category Number	Experimental Materials	Phenomenon of Waveforms Unique to Biological Electric Shocks
1	Live experimental mice	Appeared
2	Non-living fresh meat (approximately 75% water content)	Appeared
3	Low water content fresh meat (approximately 6% water content)	Not appeared
4	Wood that has been soaked in a sodium chloride aqueous solution	Appeared
5	Wood that has been soaked in a glycerol solution containing sodium chloride	Not appeared

2.2. The Mechanism by Which the Electrolysis of Water Affects Body Impedance

The primary reason for conductivity in biological tissues is the presence of freely moving charged particles (such as sodium ions and chloride ions) in the body's aqueous solutions. The observed decrease in body impedance upon electric shock indicates an increase in the concentration of these charged particles within the body's conductive fluids during the shock. Having established that water is a key factor, further exploratory experiments are conducted to investigate the specific causes of this phenomenon. Additionally, since both non-living meat tissue and living animals exhibit waveforms unique to biological electric shocks, we chose to conduct an in-depth study of this phenomenon using non-living meat to minimize animal harm.

According to electrochemical theory, when the voltage applied between electrodes in water exceeds the minimum voltage required for the water electrolysis reaction, the electrolysis of water will occur, decomposing water molecules into hydrogen and oxygen [20]. The following experiment is designed to observe if water electrolysis occurs within meat when an electric shock is applied. The experimental structure is shown in Figure 7. The effective voltage between the electrodes is set at 70 V. A high-precision hydrogen detector is used to monitor hydrogen production directly above the electrodes, verifying if electrolysis occurs during the experiment. This hydrogen detector displays hydrogen concentration in parts per million (ppm) by mole. Additionally, a gas collection hood is employed to minimize the impact of hydrogen diffusion on the experimental results.

The changes in hydrogen concentration monitored by the detector during the experiment are shown in the upper part of Figure 7. After a period of electrification, the detector recorded a continuous increase in hydrogen concentration. This indicates that an electrolysis reaction occurred within the body during the electric shock. Additionally, we measured the mass of the electrically shocked body before and after the shock using a high-precision mass measurement device. We conducted four sets of experiments, and the results are shown in Table 2. In four experiments, the mass of electrically shocked body decreased to varying degrees, indicating that substance loss occurred during the electric shock process. This finding strongly supports the view that electrolysis of water occurs within the body during the electric shock. The above results confirm the fact that electrolysis of water occurs within the body during an electric shock.

Table 2. Statistics of mass changes in electrically shocked bodies before and after experiments.

Team Number	Pre-Experiment Mass (g)	Post-Experiment Mass (g)	Magnitude of Mass Reduction (g)
1	40.236	40.164	0.072
2	40.082	39.993	0.089
3	53.073	52.864	0.209
4	50.488	50.320	0.168

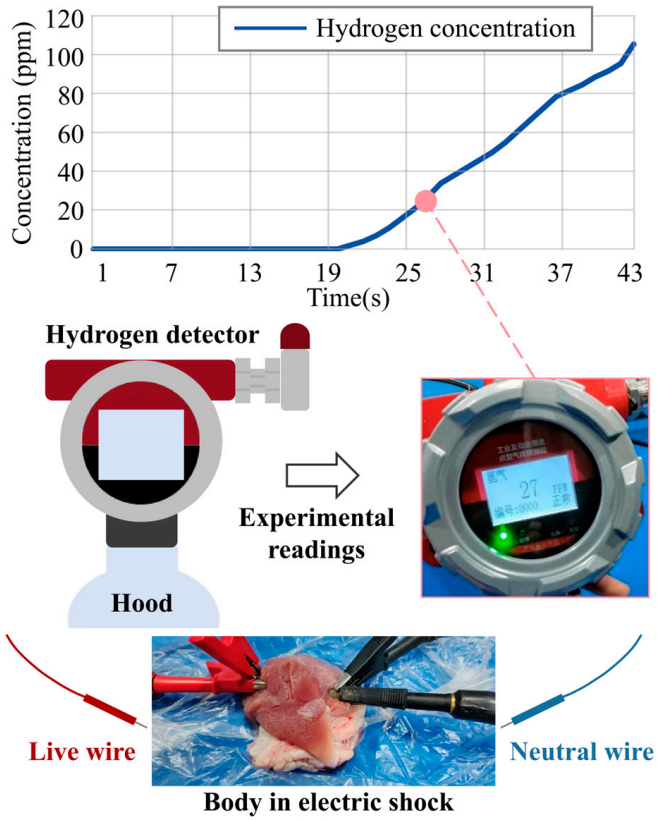

Figure 7. Graph of the process of increasing hydrogen concentration during the experiment.

In summary, we have qualitatively explained the phenomenon of waveforms unique to biological electric shocks. When an electric shock occurs, water molecules within the animal's body undergo electrolysis due to the applied voltage. The decomposition of water molecules increases the concentration of ions in the solution, raising the conductivity and lowering the resistance. After a period of time, the resulting oxygen and hydrogen gases struggle to dissipate promptly due to the meaty structure of the organism, accumulating near the electrodes and affecting the subsequent reaction process. This slows down the rate of water decomposition, leading to a gradual slowdown in the decrease of resistance. The phenomenon of waveforms unique to biological electric shocks is related to the electrolysis of water. In Section 3, we develop a mathematical model to quantitatively analyze the aforementioned process.

3. Impedance Modeling of Animal Bodies Based on Quantifying the Impact of Water Electrolysis

Based on the qualitative analysis of the relationship between water electrolysis and animal body impedance, we developed a quantitative animal impedance model that accounts for the impact of water electrolysis.

3.1. The Mathematical Relationship Between Water Electrolysis and the Dynamic Resistance of an Electrically Shocked Body

According to the chemical equation for water electrolysis, the ratio of hydrogen molecules to water molecules is 1:1. Therefore, the rate of hydrogen production v_H is numerically equal to the rate of water decomposition v_w.

If the gas bubbles produced during water electrolysis are not promptly expelled and instead adhere to the electrodes, they can impede the reaction process and gradually decrease the reaction rate [21–23]. In an electrically shocked body, the internal aqueous solution permeates the tissue, and the structure of the tissue obstructs the expulsion of the generated gases. Consequently, the rate of water electrolysis within the body decreases

over time. Simultaneously, the change in impedance of the electrically shocked body within a unit of time also diminishes. By setting the ratio of the water decomposition rates at adjacent moments to a fixed value, we can describe the gradual decline in reaction rate. Based on actual measured data showing a gradual slowdown in the impedance reduction rate, this ratio is set to 1.0019. Therefore, the mathematical expression for the water decomposition rate v_w at time t is given by (1).

$$v_w(t) = \frac{v_w(t-1)}{1.0019} \tag{1}$$

The unit of v_w(t) is L/s. The initial water decomposition rate, $v_w(0)$, is a model parameter that needs to be set in advance. Additionally, based on the solution volume and the rate of water decomposition, the expression for the solution volume $V(t)$ at time t can be derived, as shown in (2).

$$V(t) = V(t-1) - v_w(t-1) \tag{2}$$

The unit of $V(t)$ is L. The model parameter $V(0)$ represents the initial solution volume and should be set in advance. Additionally, the reduction in solution volume will lead to an increase in solution concentration. Thus, the expression for the solution concentration $C(t)$ at time t can be derived, as shown in (3).

$$C(t) = \frac{V(0)C(0)}{V(t)} \tag{3}$$

The terms $V(0)$ and $C(0)$ in the equation represent the initial volume and concentration of the aqueous solution, respectively. The numerator indicates the amount of substance of the solute in the solution, while the denominator represents the volume of the solution. Their ratio, $C(t)$, denotes the concentration of the solution at time t, with units in mol/L. At this point, the mathematical relationship between solution concentration and time has been established. As the concentration of salt in the aqueous solution increases, the solution's conductivity will also increase. According to the [24], the relationship between the salt concentration C and the conductivity σ of the aqueous solution can be obtained, as shown in (4).

$$\sigma(t) = 88.35C(t) + 1.775 \tag{4}$$

Equation (4) represents the mathematical relationship between the molar concentration (mol/L) of a salt solution and its conductivity (mS/cm) at time t. The average length of the electrically shocked body is l, in centimeters (cm), and the average cross-sectional area is S, in square centimeters (cm^2). Thus, the expression for the dynamic resistance R_S within the electrically shocked body is shown in (5).

$$R_S(t) = \frac{l}{S \cdot \sigma(t)} \tag{5}$$

In (5), the equivalent cross-sectional area and equivalent length of the conductive body are constant, while only the conductivity changes over time, causing the resistance to vary with time.

The mathematical relationships between the various intermediate variables in the water electrolysis process have been obtained. By integrating (1) through (5) to express dynamic resistance as the dependent variable with time as the independent variable, we derive an expression for the relationship between dynamic resistance R_S and time t, as shown in (6).

$$R_S = \frac{l}{S\left(\frac{88.35V(0)C(0)}{V(0)-\int_0^t \frac{v_w(0)}{1.0019^t}dt} + 1.775\right)} \tag{6}$$

Among them, l, S, $V(0)$, $C(0)$ and $v_w(0)$ are model parameters that need to be assigned values based on actual conditions before running the model.

3.2. Considering the Time-Varying Resistance Characteristics of the Animal Body Impedance Model

Based on the above theory, a schematic diagram of the activity of relevant microscopic particles within an animal's body during electric shock is shown in Figure 8. Using laboratory mice as an example, we consider the electric shock current path as "skin–body–skin". According to the traditional equivalent approach, which takes into account the capacitive and resistive characteristics of the skin epidermis, we model the skin section as a parallel combination of resistance and capacitance. The internal current primarily flows through the directional movement of ions in body's aqueous solutions.

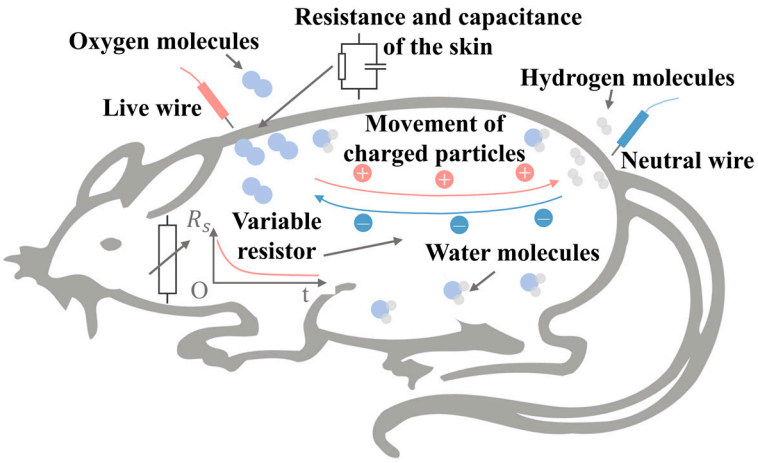

Figure 8. Schematic diagram of microscopic particle activity in an animal's body during electric shock.

Based on the mathematical rules of the dynamic resistance of the conductive parts containing water within the body, an animal body impedance model that considers the time-varying characteristics of internal resistance is established. The circuit structure is shown in Figure 9. This circuit structure represents the topological form of WEDI model.

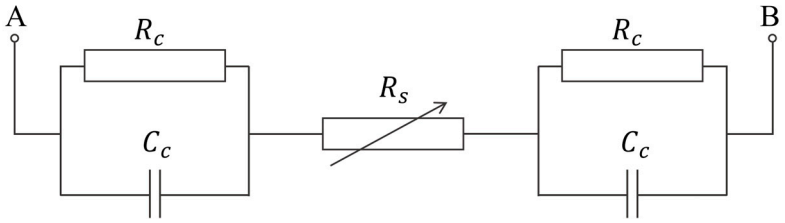

Figure 9. The topological diagram of the WEDI model.

In this diagram, points A and B are the contact points of the external electrodes. The R_c represents the skin resistance. The C_c represents the skin capacitance. The frequency of the contact voltage is denoted by f. The dynamic resistance R_s follows the variation pattern described by (6). Based on the circuit structure shown, the relationship between the impedance Z of the animal body and time t upon electric shock can be derived as shown in (7).

$$Z = \frac{l}{S\left(\frac{88.35V(0)C(0)}{V(0)-\int_0^t \frac{v_w(0)}{1.0019^t}dt} + 1.775\right)} + \frac{2R_c}{1+(2\pi f C_c R_C)^2} - \frac{4\pi f C_c R_c^2}{1+(2\pi f C_c R_C)^2} j \quad (7)$$

Equation (7) describes the relationship between the impedance of a body experiencing electric shock and the duration of the shock, representing the mathematical form of the WEDI model. Before running the WEDI model, several parameters need to be set: initial water decomposition rate $v_w(0)$, initial total volume of the aqueous solution $V(0)$, initial concentration of the solution $C(0)$, average length l and cross-sectional area S of the body, skin capacitance C_c, skin resistance R_c, and frequency of the applied voltage f.

The flowchart of the WEDI model's operation is shown in Figure 10.

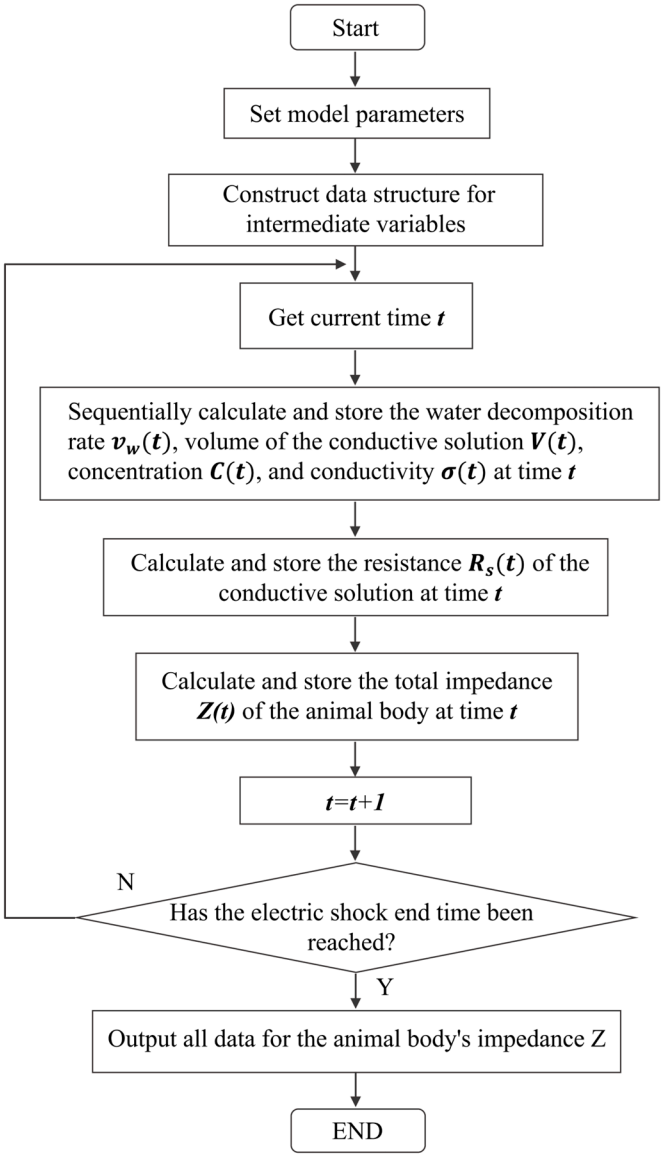

Figure 10. The program flow diagram of the WEDI model.

First, set the model parameters before running the simulation: the initial water decomposition rate $v_w(0)$, the initial total volume of the solution $V(0)$, the initial concentration of the solution $C(0)$, the average length of the electrical conductor l, the average cross-sectional area S, skin capacitance C_c, skin resistance R_c, the frequency of the electric shock voltage f, and the end time of the electric shock t_e.

Next, create multiple one-dimensional arrays indexed by time for intermediate variables: $v_w(t)$, $V(t)$, $C(t)$, and $\sigma(t)$ to store the values of each variable at each time step. Then calculate the dynamic resistance $R_s(t)$ and the total impedance of the animal body $Z(t)$.

Finally, increment the time t by one model time unit for the next round of calculations. The relationship between the time variable t and real-world time is that each increment

of t corresponds to a passage of 0.0001 s in real time. The program will check whether the current time t has reached the end time of the electric shock t_e. If not, it will restart the calculation; if it has, the program will exit and output the impedance array Z. The data sequence in array Z represents the real and imaginary components of impedance at each moment during the electric shock, thoroughly detailing the changes in the animal's impedance throughout the process.

Thus, the reduction of water molecules within the animal's body due to electrolysis, which leads to an increase in the concentration of the solution and subsequently an increase in conductivity, is captured through mathematical expressions. The variations in internal resistance based on the changes in conductivity are derived, and a mathematical model of the animal's impedance over time is established, considering the effects of water electrolysis.

4. Verification and Comparative Analysis of the WEDI Model

We used the established WEDI model to calculate the electric shock current in mice and compared the results with measured electric shock current data to verify validity of the proposed model. Additionally, we compared the WEDI model with existing bioimpedance models to demonstrate the advanced nature of the proposed model.

4.1. Construction of a Low-Voltage Electric Shock Real-Type Experimental Platform

We constructed a low-voltage electric shock real-type experimental platform, as shown in Figure 11. A programmable power supply outputs a stable 220 V sine wave voltage to simulate mains electricity. The single-phase isolation transformer ensures the safety of experimental operators. The NI data acquisition system, equipped with built-in data acquisition boards, can collect voltage and current data during the experiment at a sampling rate of 10 kHz. Strong alligator clips ensure full and stable contact between the shock electrodes and the test subject. The test subjects are live laboratory mice specifically used for experiments. Additionally, the animal experiments involved in this study have been approved by the institution's Ethics Committee.

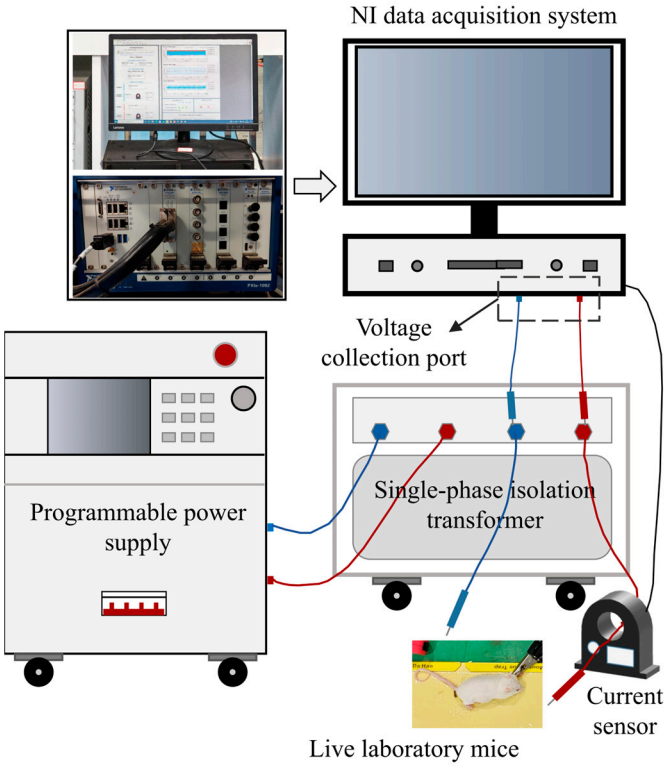

Figure 11. The structure diagram of a low-voltage electric shock real-type experimental platform.

4.2. Validation of the WEDI Model

We conducted an electrical shock experiment on live lab mice using an AC voltage with an effective value of 220 V and collected real electrical current data during the shocks. At the same time, we used the WEDI model to calculate the electrical current experienced by the lab mice during the shocks. Before running the WEDI model, we assigned values to the model parameters based on the specific electric shock scenario.

The initial water decomposition rate is set at 2.8276×10^{-5} L/s, based on [25,26]. The total volume of the aqueous solution at the initial moment is set at 2×10^{-2} L, calculated according to the body mass and water content of mice. The initial concentration of the solution is set at 1.15×10^{-1} mol/L, reflecting the sodium chloride concentration within the mice's bodies. The average length and average cross-sectional area of the electrode are set at 15 cm and 2 cm^2, respectively, based on actual measurements. The skin capacitance of the electrode is set at 2.2×10^{-7} F, based on [27]. The skin resistance of the electrode is set at 1150 Ω, determined through actual measurement. The applied voltage frequency is set at 50 Hz.

After completing the assignment, we start running the WEDI model to calculate the electric shock current in laboratory mice under experimental conditions. We compare the model calculation results with the actual measured data from live experiments, as shown in Figure 12. The moment at 0.02 s marks the first instance of electric shock. The blue line represents the electric shock current waveform calculated by the model, while the red line indicates the actual measured electric shock current waveform. As shown in the figure, both the model-calculated waveform and the measured waveform exhibit a trend where the amplitude initially increases before stabilizing, and they demonstrate a high degree of conformity.

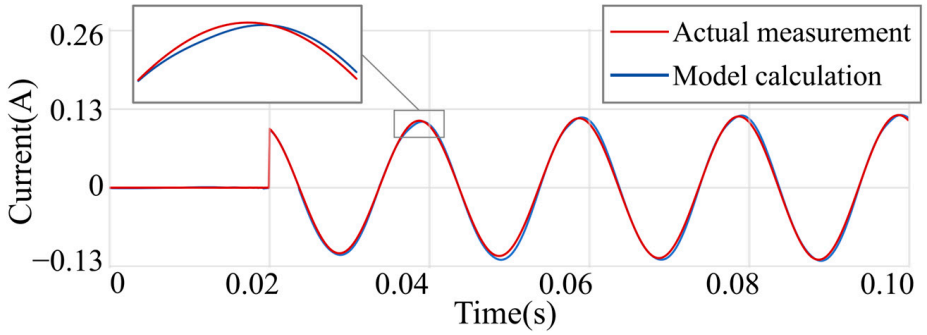

Figure 12. Comparison of the electric shock current waveforms calculated by the WEDI model to those actually measured.

Simultaneously, Mean Absolute Percentage Error (MAPE), Mean Absolute Error (MAE), and Root Mean Square Error (RMSE) serve as metrics to quantify the error between the model output data sequence and the measured data sequence. An error analysis is conducted by comparing the WEDI model output data with the measured data. The values for the metrics MAPE, MAE, and RMSE are 0.00357, 0.00350, and 0.00446, respectively.

4.3. Comparison and Analysis with Existing Research

We reproduced three existing classical bioimpedance models (sourced from references [11,12,19], and calculated the electric shock current of mice in the aforementioned true-to-scale electric shock experimental scenario. The comparison between the calculated results and the measured data is shown in Figures 13–15.

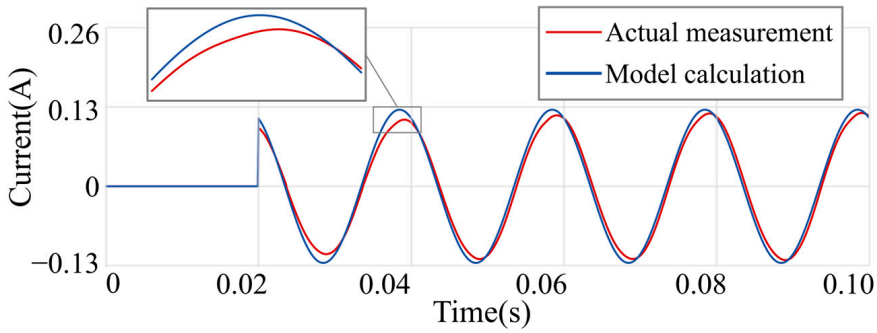

Figure 13. Comparison of the electric shock current waveforms calculated by the model in [11] to those actually measured.

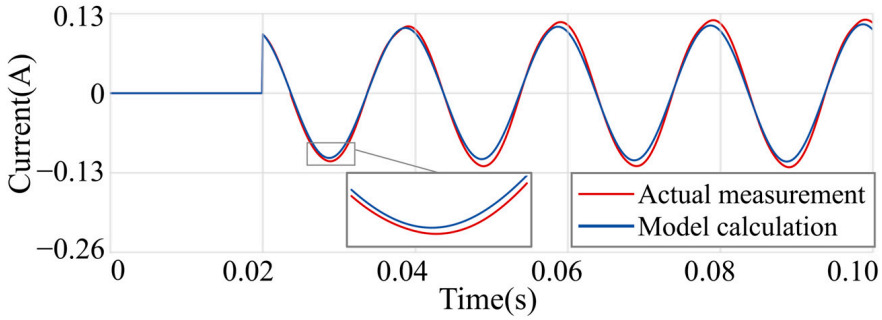

Figure 14. Comparison of the electric shock current waveforms calculated by the model in [19] to those actually measured.

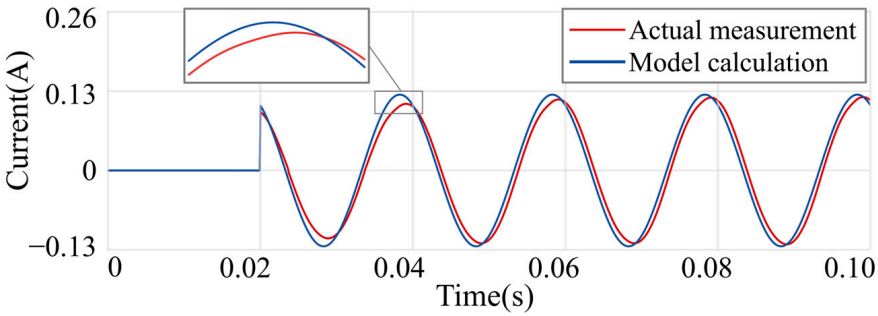

Figure 15. Comparison of the electric shock current waveforms calculated by the model in [12] to those actually measured.

Based on the output waveform of electric shock current, it is evident that the models from references [11,12] produce a constant amplitude of electric shock current. Although the output waveforms of these models align closely with the measured waveform in the later stage, there is a significant discrepancy during the initial phase, making it difficult to reflect the time-varying characteristic of body impedance during electric shock. On the other hand, the model from [19] shows an increasing trend in the electric shock current during the initial phase. This indicates that the model captures the time-varying property of body impedance, although some differences with the measured waveform still exist. Furthermore, Table 3 presents the comparison metrics for the WEDI model and three existing models. The WEDI model has the lowest values for all three error metrics. Therefore, the comparison of output waveforms and related metrics demonstrates that the WEDI model is more accurate than traditional models.

Table 3. Comparative analysis of existing models.

Metrics	WEDI	[11]	[19]	[12]
Mean Absolute Percentage Error	0.00357	0.01002	0.00653	0.01408
Mean Absolute Error	0.00350	0.01000	0.00642	0.01404
Root Mean Square Error	0.00446	0.01095	0.00757	0.01528

In addition, the models in [11,12] are constructed based on a combination of fixed resistors and capacitors. Such models struggle to explain the time-varying characteristics of body impedance during electric shock. On the other hand, the model in [19] is developed by fitting the waveform of electric shock current and can describe the impedance variation pattern. Although this model reflects the time-varying characteristics of body impedance at the initial stage of electric shock to some extent, it falls short in explaining the deeper mechanistic reasons for impedance changes. The WEDI model, however, is built upon the observed fact that the electrolysis of water induces time-variant body impedance during electric shock. It integrates mathematical relationships among multiple variables in the electrolysis process and provides a theoretical explanation for the transition of body impedance from high to low and its subsequent stabilization.

In summary, comparative analysis shows that the WEDI model is more accurate than existing models. Additionally, it offers enhanced interpretability, as it can explain the phenomenon of waveforms unique to biological electric shocks from a mechanistic perspective.

5. Conclusions

This study examines the intrinsic mechanism underlying the time-varying body impedance in animals subjected to low-voltage electric shock. Our mechanistic analysis reveals that this phenomenon is primarily driven by the electrolysis of water within the animal's body.

- Mechanistic Explanation: We identified that the electrolysis of water molecules, induced by an electric field, leads to a reduction in water molecule concentration and an increase in conductive ion concentration in bodily fluids. This heightened ion concentration enhances electrical conductivity, resulting in decreased body impedance.
- Dynamic Impedance Model Development: Based on the electrolysis mechanism, we developed a dynamic impedance model that calculates changes in impedance over time. The model integrates relationships among solution concentration, electrical conductivity, and body impedance, providing a comprehensive framework for understanding impedance variations during electric shock.
- Model Validation: The WEDI model demonstrated strong predictive accuracy with a Mean Absolute Percentage Error of 0.00357, a Mean Absolute Error of 0.00350, and an Root Mean Square Error of 0.00446 when compared to experimental data.

These findings not only elucidate the mechanisms behind time-varying impedance in shocked animals but also present a robust model for predicting impedance changes, significantly contributing to our understanding of the principles underlying waveforms unique to biological electric shocks.

Author Contributions: Conceptualization, H.T. and X.Z.; methodology, H.T.; software, H.T.; validation, H.T., K.Y. and Z.Z.; formal analysis, X.Z.; investigation, H.T.; resources, X.Z.; data curation, K.Y.; writing—original draft preparation, H.T.; writing—review and editing, Z.Z.; visualization, H.T.; supervision, X.Z.; project administration, K.Y.; funding acquisition, X.Z. and H.T. All authors have read and agreed to the published version of the manuscript.

Funding: This research was funded by the National Natural Science Foundation of China under Grant 52037001 (Funder: National Natural Science Foundation of China) and the Postgraduate Scientific Research Innovation Project of Hunan Province under Grant CX20220858 (Funder: Hunan Provincial Department of Education).

Data Availability Statement: Our data is required to be kept confidential. Therefore, we are currently unable to make it publicly available.

Conflicts of Interest: The authors declare that they have no known competing financial interests or personal relationships that could have appeared to influence the work reported in this paper.

References

1. Li, T.; Huang, W.; Qiu, Z. Analysis on public safety of low-voltage distribution network. *Distrib. Util.* **2021**, *38*, 9–14. (In Chinese) [CrossRef]
2. Ye, H.; Li, C.; Gao, G.; Wang, H.; Ren, P. Experiment and analysis of animal electric shock current characteristics based on multiple factors. *J. Jiangsu Univ. (Nat. Sci. Ed.)* **2020**, *41*, 39–45. (In Chinese) [CrossRef]
3. Parise, G. A new summary on the IEC protection against electric shock. *IEEE Trans. Ind. Appl.* **2013**, *49*, 1004–1011. [CrossRef]
4. Zhao, H.; Xiao, X.; Sun, Q. Identifying Electric Shock in the Human Body via α Dispersion. *IEEE Trans. Power Deliv.* **2018**, *33*, 1107–1114. [CrossRef]
5. Czapp, S.; Borowski, K. Verification of safety in low-voltage power systems without nuisance tripping of residual current devices. *Electr. Power Syst. Res.* **2019**, *172*, 260–268. [CrossRef]
6. Xu, H.; Wang, X.; Wei, Y.; Zhao, Q. Dynamic impedance analysis of live electrocution based on least squares method. *J. Electr. Eng.* **2023**, *18*, 268–276. (In Chinese) [CrossRef]
7. Bridges, J.E.; Vainberg, M.; Wills, M.C. Impact of recent developments in biological electrical shock safety criteria. *IEEE Trans. Power Deliv.* **1987**, *2*, 238–248. [CrossRef]
8. Lukaski, H.C. Biological indexes considered in the derivation of the bioelectrical impedance analysis. *Am. J. Clin. Nutr.* **1996**, *64*, 397S–404S. [CrossRef]
9. Foster, K.R.; Lukaski, H.C. Whole-body impedance--what does it measure? *Am. J. Clin. Nutr.* **1996**, *64*, 388S–396S. [CrossRef]
10. De Santis, V.; A Beeckman, P.; Lampasi, D.A.; Feliziani, M. Assessment of human body impedance for safety requirements against contact currents for frequencies up to 110 MHz. *IEEE Trans. Biomed. Eng.* **2010**, *58*, 390–396. [CrossRef]
11. Chinen, K.; Kinjo, I.; Zamami, A.; Irei, K.; Nagayama, K. New equivalent-electrical circuit model and a practical measurement method for human body impedance. *Bio-Medi. Mater. Eng.* **2015**, *26*, S779–S786. [CrossRef]
12. Bora, D.J.; Dasgupta, R. Estimation of skin impedance models with experimental data and a proposed model for human skin impedance. *IET Syst. Biol.* **2020**, *14*, 230–240. [CrossRef]
13. Freschi, F.; Guerrisi, A.; Tartaglia, M.; Mitolo, M. Numerical simulation of heart-current factors and electrical models of the human body. *IEEE Trans. Ind. Appl.* **2013**, *49*, 2290–2299. [CrossRef]
14. Ferreira, D.M.; Silva, C.S.; Souza, M.N. Electrical impedance model for evaluation of skin irritation in rabbits and humans. *Ski. Res. Technol.* **2007**, *13*, 259–267. [CrossRef]
15. Li, C.; Ye, H.; Wang, C.; Wang, H. Human electric shock law based on pig electric shock experiment. *J. Jiangsu Univ. (Nat. Sci. Ed.)* **2019**, *40*, 553–558+565. (In Chinese) [CrossRef]
16. Li, C.; Wang, H.; Zhang, Y.; Du, S.; Ye, H.; Gao, G.; Luo, J. Construction and verification of 3D electrical model of pig body. *Trans. Chin. Soc. Agric. Eng.* **2019**, *35*, 185–193. (In Chinese) [CrossRef]
17. Dorgan, S.; Reilly, R.; Dorgan, S.; Reilly, R. A model for human skin impedance during surface functional neuromuscular stimulation. *IEEE Trans. Rehabilitation Eng.* **1999**, *7*, 341–348. [CrossRef]
18. Pritchard, G. A new model for human body impedance. *IEEE Trans. Power Deliv.* **2021**, *37*, 955–959. [CrossRef]
19. Yang, G.; Quan, S.; Gao, W. A new-designed biological electric shock identification method in low-voltage distribution network. *IEEE Trans. Power Deliv.* **2022**, *38*, 1558–1568. [CrossRef]
20. Millet, P.; Ngameni, R.; Grigoriev, S.; Mbemba, N.; Brisset, F.; Ranjbari, A.; Etiévant, C. PEMPEM water electrolyzers: From electrocatalysis to stack development. *Int. J. Hydrogen Energy* **2009**, *35*, 5043–5052. [CrossRef]
21. Higuera, F. A model of the growth of hydrogen bubbles in the electrolysis of water. *J. Fluid Mech.* **2021**, *927*, A33. [CrossRef]
22. Liu, H.; Pan, L.-M.; Huang, H.; Qin, Q.; Li, P.; Wen, J. Hydrogen bubble growth at micro-electrode under magnetic field. *J. Electroanal. Chem.* **2015**, *754*, 22–29. [CrossRef]
23. Liu, H.; Pan, L.; Wen, J. Numerical simulation of hydrogen bubble growth at an electrode surface. *Can. J. Chem. Eng.* **2015**, *94*, 192–199. [CrossRef]
24. Liu, P. The Study on Conductance Method of Salinity in High Salinity Wastewater. Master's Thesis, College of Geography and Environment, Shandong Normal University, Jinan, China, 2016. (In Chinese).
25. Clary, K.E.; Karayilan, M.; McCleary-Petersen, K.C.; Petersen, H.A.; Glass, R.S.; Pyun, J.; Lichtenberger, D.L. Increasing the rate of the hydrogen evolution reaction in neutral water with protic buffer electrolytes. *Proc. Natl. Acad. Sci. USA* **2020**, *117*, 32947–32953. [CrossRef]

26. Mi, L. Study on the Influence of Blade Tip Structure Change on Flow Field Characteristics of Wind Turbine. Master's Thesis, Mechanical & Electrical Engineering Institute, Xinjiang Agricultural University, Urumqi, China, 2021. (In Chinese).
27. Li, K.; Wang, C.; Wang, Y.; Wu, Y. Fault leakage current characteristics and protection methods of single-phase power supply and consumption system. *J. Tiangong Univ.* **2023**, *42*, 63–70. (In Chinese) [CrossRef]